Indonesian Journal of Physics
Vol 16 No. 4, October 2005

VLF Data Analysis Through Transformation Into Resistivity Value: Application tTo Synthetic and Field Data

Wahyu Srigutomo[1)], Asep Harja[1)], Doddy Sutarno[1)], and Tsuneomi Kagiyama[2)]
[1)]Electromagnetic Induction Lab., Department of Physics,
Faculty of Mathematics and Natural Sciences,
Institut Teknologi Bandung
[2)]Aso Volcanological Lab., Institute for Geothermal Science,
Grad. School of Science, Kyoto University
e-mail: wahyu@fi.itb.ac.id

Abstract

Transformation of VLF-EM signals, which are approximated as the real and imaginary components of the ratio between the vertical and the horizontal components of magnetic fields was carried out in this study to improve the quantitative interpretation aspect of VLF analysis. The transformation filter has been tested using synthetic data generated by a two-dimensional finite element algorithm that provides VLF responses for several models typically encountered in VLF surveys. The transformed apparent resistivity profiles show good agreement in value and pattern to those modeled by the finite element algorithm. The transformation was applied to the field data and further analysis was conducted by inverting the recorded original VLF-EM signals and the transformed apparent resistivity into a two-dimensional resistivity-depth section. From the comparison with the dc-resistivity-depth section obtained previously, the resulted resistivity section revealed the general features of the subsurface structure.

Keywords: *VLF-EM signals; apparent resistivity; transformation filter; two-dimensional resistivity-depth section*

1. Introduction

The Very Low Frequency (VLF) method is an inductive exploration method that measures variation in EM field components related to the electrical structure of the subsurface. The method utilizes source of EM signals propagated by a remote transmitter (vertical electric dipole) within the frequency range of 15 to 30 kHz. VLF transmitters, which are mainly established to serve communication among naval submarines, radially transmit primary EM fields that consist of a horizontal magnetic field component H_φ and a vertical electric field component E_z perpendicular to the direction of propagation. At large distances from the transmitter (> several free-space wavelengths), the primary EM fields can be regarded as plane waves. Due to the interaction with the local subsurface conductivity, the primary horizontal magnetic field (now approximated by H_y in Fig. 1a) generates a horizontal electric field E_x in the direction of propagation. Any conductivity variations whose strike is relatively parallel to the direction of propagation of the plane wave will generate secondary magnetic fields either inductively or galvanically. The measured ratios of this vertical secondary field to the total horizontal field reflect the variation of conductivity structure, allowing this method to become widely used for prospecting conductive materials since 1960's[1)], and is effectively fast and powerful for the study of geological structures to a maximum depth of about 100 m as discussed by Fischer *et.al*[2)]. Various examples of geological and hydrogeological application of this method were discussed comprehensively by McNeil and Labson[3)].

VLF methods are grouped into two types on the basis of the measured parameters. The first, which is of interest in our present study, only measures the components of the elliptically polarized magnetic field, called as VLF-EM or simply VLF method. The second deals with the horizontal electric field component and the orthogonal horizontal magnetic field, make it possible to calculate the apparent resistivity and phase of impedance at the surface. This type is called VLF-R or sometimes referred as VLF-MT method since it applies the same formulations as used in magnetotelluric (MT) method.

Despite the broadly usefulness of the VLF-EM method, interpretation of the anomalies is mainly carried out qualitatively using anomaly curves and nomograms e.g.[4-7)]. In practice, it is common to plot the real and imaginary parts of the normalized vertical field on stacked profiles and analyze the shape of the observed curves such as cross-overs and peaks which can be attributed to the presence of vertical conductor or lateral contacts of different resistivities beneath the surface. A filter to transform cross-overs into anomalous peaks was introduced by Fraser[8)] by applying a differential operator with a band-pass frequency response. Later, Pedersen *et.al*.[9)] proposed a horizontal derivative of the ratio of vertical magnetic field to the horizontal magnetic field that yields a peak directly over a conductor. Karous and Hjelt[10)] proposed a filter to obtained an equivalent current density cross-section that would give rise to the observed real (in-phase) data. This filter is a generalization of Fraser filter with the assumption that the anomalous magnetic field generated in the localized conductors is due to low-frequency current distributions through Biot-Savart's law, omitting the induction effects. The application of this filter for various subsurface models have been demonstrated by Ogilvy and Lee[11)], showing its efficiency to locate the position of the source of the anomalous field. However, all the above transformations do not yield direct

information of conductivity σ or its inverse, resistivity ρ which could be compared with data from geolectrical or other EM methods. It is important to note that recently Pedersen and Becken[12] introduced a new fast imaging technique to derive the equivalent current density distribution using the integral equation method resulting a contour that is not only sensitive to the lateral change of conductivity but also reflects the depth boundaries of the conductors, grossly mimics the conductivity structure derived from the MT inversion.

Transformation filter that transforms the measured H_z/H_y (known as tipper in MT-related subjects) into apparent resistivity profiles was first introduced by Choutea *et.al.*[13] with the assumption that the spatial derivatives of the horizontal magnetic field can be neglected along the profile. Gharibi and Pedersen[14] proposed an improvement to this method by using the fact that the secondary horizontal and vertical magnetic fields are of internal origin and form a Hilbert transform pair. This method enables one to obtain the impedance tensor from the magnetic fields.

In this study, we applied the transformation of VLF-EM signals into apparent resistivity profiles based on the above two transformation schemes. 2D finite element method was employed to several models to obtained electric field responses. The vertical and horizontal components of magnetic field were then calculated using differential relation of the Maxwell's equations. Having a complete set of EM field responses (electric and magnetic fields), the apparent resistivity value can be easily obtained. In the mean time, the tipper resulted from the modeling scheme, approximated as the parameters observed in VLF-EM method, was transformed to obtain the apparent resistivity value. Comparisons of the transformed apperent resistivities with those calculated from the 2D modeling are presented in this paper. Finally, the transformation scheme was used to the field VLF data collected at two lines in Baleendah, south of Bandung. 2D inversion was applied to the original VLF data and the transformed apparent resistivity to obtain resistivity cross-section. Comparison with the resistivity structures inverted from DC resistivity data was made also to evaluate the effectiveness of the overall workflow in obtaining information of the subsurface structure.

2. VLF-EM Parameters

Figure 1a describes the configuration of a preferred VLF survey. The survey lines are approximately parallel to the incident magnetic field (*y*-axis) and at right angles to the geological strike of conductor (transverse electric [TE] mode) and to the direction of transmitter location (*x*-axis). Due to the presence of conductive inhomogeneity, secondary fields generated by the induced current are superimposed on the primary field, resulting in a total field that is elliptically polarized (Fig. 1b). The tilt angle α, which is the inclination of the major axis of the polarization ellipse, and the ellipticity ε, which is the ratio of the minor to the major axis of the ellipse, are calculated by the formulas[15]

$$\tan\alpha = \pm\frac{2\left(H_z/H_y\right)\cos\Delta\phi}{1-\left(H_z/H_y\right)^2} \tag{1}$$

and

$$\varepsilon = \frac{H_z H_y \sin\Delta\phi}{H_1^2}, \tag{2}$$

where H_z and H_y are the vertical and horizontal components of the total magnetic field; $\Delta\phi = \phi_z - \phi_y$ is the phase difference, where ϕ_z and ϕ_y are the phases of the vertical and horizontal magnetic field components; and

$$H_1 = \left|H_z e^{i\Delta\phi}\sin\alpha + H_y\cos\alpha\right|. \tag{2a}$$

The tangent of the tilt angle and ellipticity are good approximations to the real and quadrature components of the tipper, respectively[16]. They are often expressed in percentage as the real (= tan α x 100%) and the imaginary (= ε x 100%) anomalies which will be the focus of our study.

For comparison, a VLF-R survey deals with the horizontal electric field component and the orthogonal horizontal magnetic field. The apparent resistivity (in Ωm) is computed through the formula[17]

$$\rho_a = \frac{1}{\mu\omega}\left|\frac{E_x}{H_y}\right|^2 = \frac{1}{\mu\omega}\left|Z_{xy}\right|^2 \tag{3}$$

or

$$Z_{xy} = \left(i\omega\mu\right)^{1/2}, \tag{3a}$$

where $\mu = \mu_0$ is the magnetic permeability of the free space, ω is the angular frequency of the measurement, and Z_{xy} is the surface impedance for the TE mode.

3. Transformation into apparent resistivity

3.1 Approximate solution

As mentioned, our objective is to transform the VLF-EM signals into apparent resistivity such that of the VLF-R or MT methods. Consider a right-hand Cartesian system in a 2D earth model (positive z-axis pointing downward in Fig. 1a). The behaviour of EM fields at any frequency is concisely depicted by the Maxwell's equations. For a source free region within the Earth, negligible time varying displacement currents, and negligible variations in electrical permittivities and magnetic permeabilities of rocks compared with variations in bulk rock conductivity, the equations take the forms of

$$\nabla\times\mathbf{E} = -\frac{\partial\mathbf{B}}{\partial t} \tag{4a}$$

$$\nabla\times\mathbf{H} = \sigma\mathbf{E} \tag{4b}$$

$$\nabla\cdot\mathbf{B} = 0 \tag{4c}$$

$$\nabla\cdot\mathbf{E} = 0 \tag{4d}$$

where **E** is the electric field (in Vm^{-1}), **B** is the magnetic induction (in T), **H** is the magnetic intensity, and σ is the conductivity of the medium (in Sm^{-1}).

In a 2D TE mode, there are no field variations along the x-axis so the eq. (4a) is reduced to

$$\frac{\partial E_x}{\partial y} = \frac{\partial B_z}{\partial t}. \tag{5}$$

or

$$\frac{\partial E_x}{\partial y} = i\omega\mu_0 H_z, \tag{6}$$

assuming a time dependence $e^{i\omega t}$ of the magnetic induction. Integration of eq. (6) yields

$$E_x(y) = E_x(0) + i\omega\mu_0 \int_0^y H_z(y')dy' \tag{7}$$

An approximate solution can be obtained by assuming the magnetic is constant along the y-axis[13], i.e. $H_y(y) = H_0$. In this case eq. (7) can be expressed as

$$E_x(y) = E_x(0) + i\omega\mu_0 H_0 \int_0^y T(y')dy' \tag{8}$$

where T is the tipper,

$$T(y') = \frac{H_z(y')}{H_y(y')}. \tag{9}$$

Using the eq. (3) and (8), the surface impedance now can be given by

$$Z_{xy}(y) = \frac{E_x(y)}{H_y(y)} = \frac{E_x(0) + i\omega\mu_0 H_0 \int_0^y T(y')dy'}{H_0} \tag{10}$$

or

$$Z_{xy}(y) = Z_{xy}(0) + i\omega\mu_0 \int_0^y T(y')dy'. \tag{11}$$

The initial value of surface impedance at y = 0 can be provided from either VLF-R or MT.

In actual situation data is usually sampled at interval of Δy, then substituting eq. (3a) into eq. (11) and expressing it in a discrete form yields

$$\left(\rho_{j+\frac{1}{2}}\right)^{\frac{1}{2}} = -(i\omega\mu)^{\frac{1}{2}} \sum_{k=1}^{j} \left(\frac{H_z}{H_y}\right)_k \Delta y + \left(\rho_{j-\frac{1}{2}}\right)^{\frac{1}{2}}. \tag{12}$$

The negative sign appears in the right-hand side of eq. (12) after taking into account the opposite direction of z-axis used in the formulation. In addition, Chouteau *et.al*.[13] also noted that omitting the imaginary part will not significantly change the transformed apparent resistivity due to its less reliability and smaller amplitude than the real part. In this case eq. (12) becomes

$$\rho^{\frac{1}{2}}_{j+\frac{1}{2}} = -(\omega\mu)^{\frac{1}{2}} \Delta y R_j + \rho^{\frac{1}{2}}_{j-\frac{1}{2}}, \quad j = 1, n, \tag{13}$$

where R is the real part of the tipper. The computed apparent resistivity is located half a sample interval ahead of point j and the initial value for apparent resistivity can be provided from a DC resistivity measurement.

3.2 Full solution

Gharibi and Pedersen[14] generalized the previous approximation such that the impedance can be expressed in its full form, i.e.

$$Z_{xy}(y) = \frac{E_x(y)}{H_y(y)} = \frac{E_x(0) + \int_0^y i\omega\mu_0 H_z(y')dy'}{H_y(y)}, \tag{14}$$
$$= Z_{xy}(0)\frac{H_y(0)}{H_y(y)} + \frac{i\omega\mu_0 \int_0^y H_z(y')dy'}{H_y(y)}$$

by making use the fact that the secondary horizontal and vertical magnetic fields are of internal origin. The authors assumed the primary source of the horizontal magnetic field is constant along the y-axis, so that the expressions of the magnetic fields are

$$H_z = H_z^s \tag{15a}$$

and

$$H_y = H_y^p + H_y^s, \tag{15b}$$

where $H_y^p = H_0$ is a constant.

From the tipper formulation, the vertical magnetic field now can be expressed as

$$H_z(y) = H_z^s(y) = T(y)H(y) = T(y)H_0 + T(y)\tilde{H}_i\{H_z^s\}, \tag{16}$$

where the Hilbert transform that relates the secondary vertical and horizontal magnetic fields is in the form of [18]

$$\tilde{H}_i\{H_z^s\} = \frac{1}{\pi}\int_{-\infty}^{+\infty} \frac{1}{y'-y} H_z^s(y')dy' = H_y^s. \tag{17}$$

Gharibi and Pedersen[14] proposed an iterative scheme to solve the full solution. First step is to calculate the following relation:

$$H_z^s(n+1) = T(y) + T(y)\tilde{H}_i\{H_z^s\}, \tag{18}$$

where $H_0 = 1$ and $H_z(y) = T(y)$ are set as the initial values in the first iteration. Secondly, eq. (17) and eq. (15b) are applied to obtain H_y. Finally, H_y and H_z are substituted into eq. (14). The initial value $Z_{xy}(0)$ can be supplied at any location along the profile in the forms of either impedance or a pair of apparent resistivity & phase.

4. Forward modeling

4.1. Finite element method

The general 2D EM forward problem is a boundary value problem which solves Maxwell's equations subject to given boundary conditions. From eqs. (4a), (4b), and (4d) the second order differential equation of the TE mode in Fig.1 is given as

$$\frac{\partial}{\partial y}\left(\frac{1}{i\omega\mu}\frac{\partial E_x}{\partial y}\right) + \frac{\partial}{\partial z}\left(\frac{1}{i\omega\mu}\frac{\partial E_x}{\partial z}\right) - \sigma E_x = 0. \tag{19}$$

The finite element (FE) method, which is a numerical technique for obtaining approximate solutions to the problem was applied in this study via the Ritz variational technique[19]. This technique formulates the problem in terms of a functional whose minimum correspond to the governing equation under the given boundary condition. The approximate solution within the domain is obtained by minimizing the functional with respect to its variables. At the first step, the area domain is

divided into small triangular discrete elements constructed within pairs of adjacent horizontal and vertical grid lines. All these elements were connected with the other through their vertices and a node of an element must be at the vertices of its neighboring elements. The solutions we seek in the entire domain are represented at the nodes connecting all the elements. The smallest rectangular grid that constructs four triangular elements used in this study was as 10 x 10 m. The illustration of the elemental discretization for a typical model is shown in Fig. 2. The next step is to select the interpolation function which enables one to approximate the unknown solution E_x within each element, and a linear interpolation function is used in this study. The major step in FE analysis is to formulate the overall system of equations using the Ritz method. Dirichlet boundary condition is imposed at the upper boundary of the model domain by setting the value of the electric field to be of unity, whereas the homogeneous Neumann condition ($\partial E_x/\partial n = 0$) is incorporated at the other three boundaries. The final system of equations to solve is given by

$$|\mathbf{K}|\{\phi\} = \{b\}, \tag{20}$$

where $|\mathbf{K}|$ is an N x N matrix containing the algebraic expression of the problem. N is the total number of the unknown E_x or nodes, $\{\phi\}$ is an N x 1 vector whose elements are the E_x expansion coefficients sought, and $\{b\}$ is the equivalent known source vector. The symmetric, sparse and banded matrix was solved using the biconjugate-gradient method[20]. To implement the FE analysis in this study, moderate modification was carried out on the previously developed FE code for MT and long grounded wire problems[21;22]. Having solved the E_x, then the vertical and horizontal magnetic field components were obtained from eq. (4b).

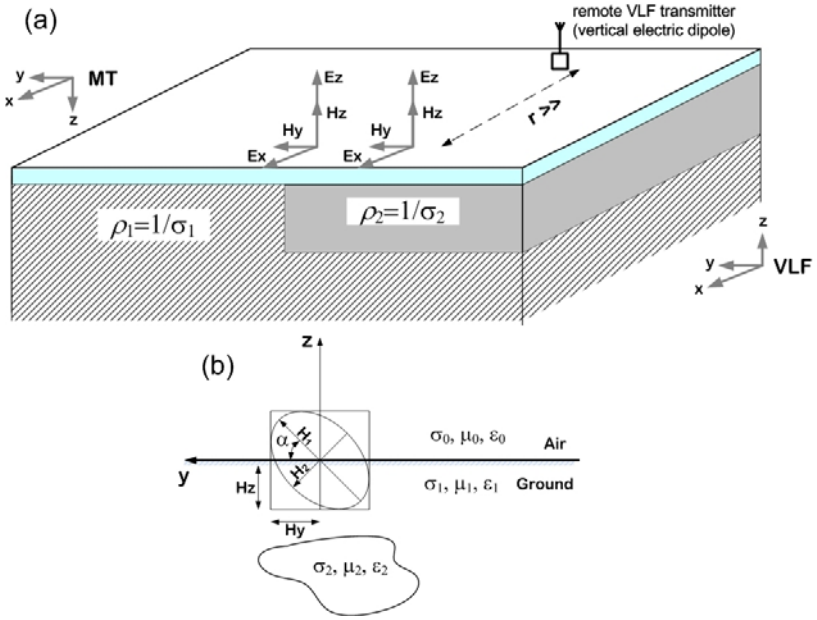

Figure 1. (a) Illustration of VLF-EM fields over inhomogeneous subsurface. (b) Polarization ellipse due to the presence of conductive inhomogeneity.

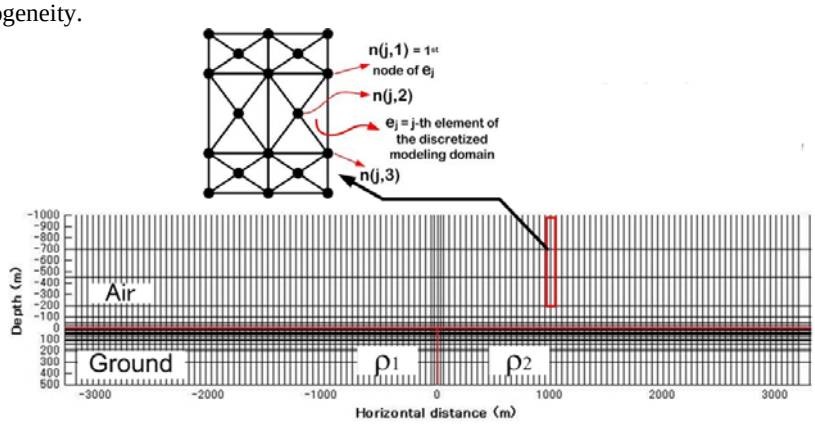

Figure 2. Typical finite element discretization used in the modeling: triangular elements

4.2 Synthetic models

VLF-EM responses of several 2D models typically encountered are calculated at 20 kHz using the above finite element scheme. The filter used for transformation from VLF signal into apparent resistivity is the approximate solution filter [eq. (12)]. The dimensions of vertical grid are mostly of 50 m except at the vicinity of the contacts, with minimum size of 10 m.

Homogeneous model

The lower panel of Fig. 3a shows a homogeneous subsurface model of 1000 Ωm. The approximate solution filter was used and the initial resistivity for the transformation was set at 1030 Ωm (3% error), which was the apparent resisitivity modeled by the FE method (apparent resisitivity that would have been measured by VLF-R or MT method). The comparison of the transformed the modeled VLF-R apparent resistivities are shown on the upper panel, indicating a good agreement in value. The tipper computed by the FE algorithm (the input of the transformation) is shown in Fig. 4a.

Vertical contact

Fig. 3b shows a subsurface model consists of two blocks of different resistivities: the left block has a resistivity of 10 Ωm; the righ block has a resistivity of 1000 Ωm and the interface is at 0 m position. It is observed also that the apparent resistivities of the FE computed and the transformed are similar. Noticeable discrepancy slightly occurs over the contact. The discrepancy appears to be attributed to the assumption in the filter that H_y is constant along the profile, which is not in the case at a contact as can be seen in Fig. 5b. The profiles in Fig. 5 are the FE computed normalized H_y for all the synthetic models, which clearly shows that H_y varies over the contact and therefore affects the associated impedance and apparent resistivity of the VLF-R or MT. The tipper for the vertical contact is shown in Fig. 4b.

Conductive dike

A vertical conductive dike of 1 Ωm is inserted between two blocks of different resistivities (10 and 1000 Ωm) as seen in Fig. 3c. The thickness of the dike is 100 m. The dike might represent an outcropping of sulphide body or a section of fractured zone in the real situation. The filtered apparent resistivity resembles that of VLF-R result. Both apparent resistivity profiles indicate the presence of the dike. As in the previous model, a discrepancy is observed over the contacts due to the variation of H_y in the real situation, as modeled in Fig. 5c. The tipper calculated for this model is presented in Fig. 4c, showing a maximum value compared to the tipper of the other models due to the presence of a highly conductive body.

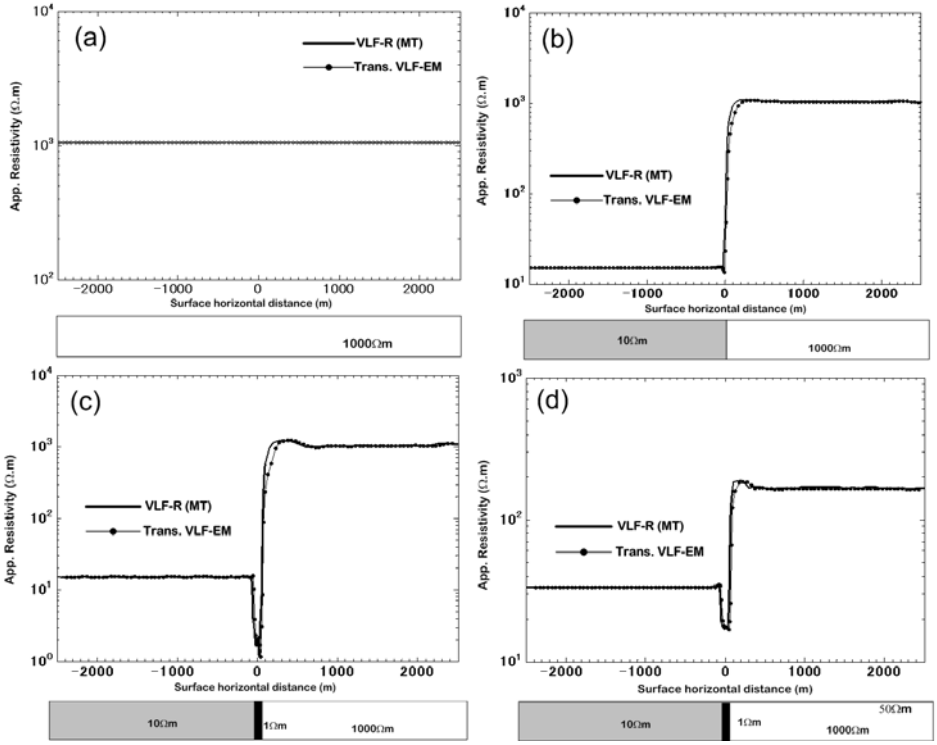

Figure 3. Basic models of subsurface resistivity in VLF-EM modeling (lower panel) and the comparison of recovered apparent resistivities resulted from the transformation filter and from the FE algorithm (upper panel). (a) Homogeneous model; ((b) vertical contact; (c) outcropping conductive dike; and (d) conductive dike under an overburden

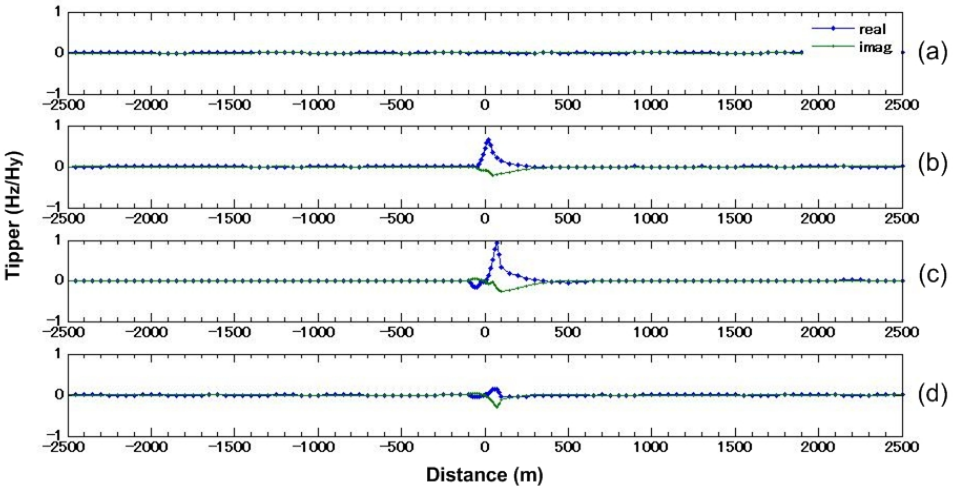

Figure 4. (a), (b), (c), and (d) are the real and imaginary parts of tipper computed by the FE algorithm for models in Fig. 3a, 3b, 3c, and 3d respectively, as inputs in the transformation.

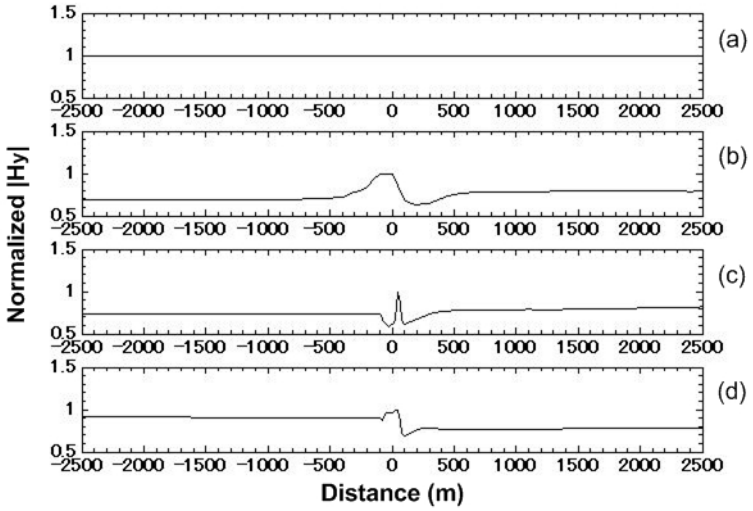

Figure 5. Normalized absolute value of H_y calculated at the surface using the FE algorithm. (a), (b), (c), and (d) are H_y profiles for models shown in Fig. 3a, 3b, 3c, and 3d, repectively.

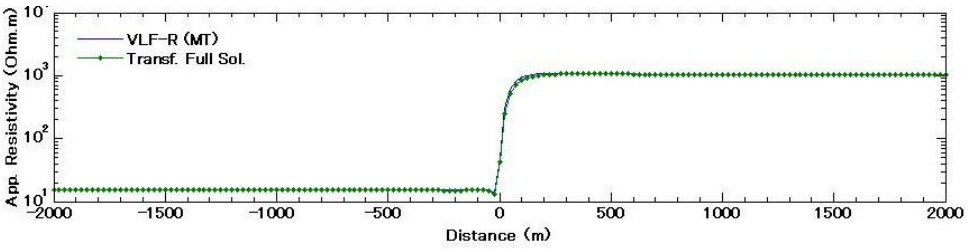

Figure 6. Apparent resistivity of a vertical contac model (Fig. 3 b) computed via FE algorithm (VLF-R) and the transformed apparent resistivity using the full solution filter.

Conductive dike under conductive overburden

A 10 m-thick of moderately conductive overburden with resistivity of 50 Ωm is now added to the model of conductive dike (Fig. 3d). The transformed apparent resistivity is similar to the FE computed apparent resistivity (VLF-R). The lowest apparent resistivity value recovered is 17 Ωm （over the dike, whereas the highest is 190 Ωm For this model, although the presence of the overburden masks the information of the structure, the overall apparent resistivity still pronounces the structure well. The profile of tipper that would be measured at the surface for this model is shown by Fig. 4d, which significantly decreases as compared with model with no overburden (Fig. 4c).

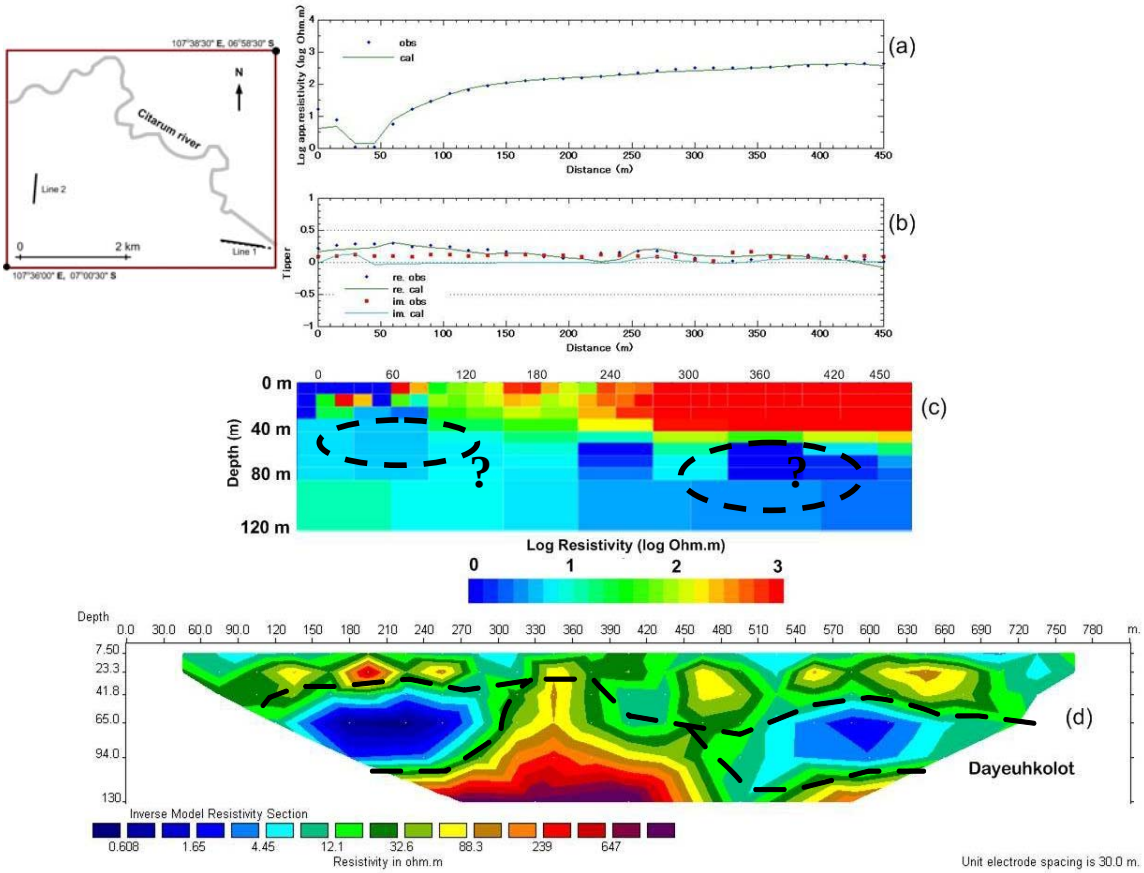

Figure 7. Upper-left panel is the map of VLF-EM and dc resistivity profiles in sub-district Baleendah, south of Bandung. (a) Solid circles is the transformed apparent resistivity from the observed VLF signals in Line 1; solid line is the inverted apparent resistivity from the Occam inversion. (b) The observed real and imaginary components the tipper (solid circles and rectangles, respectively) and the calculated signal from the inversion (solid lines). (c) 2D resistivity model inverted from the observed tipper and apparent resistivity. (d) 2D resistivity model obtained from inversion of a 2D Wenner-Schlumberger configuration.

Response of the full solution filter

The full solution of the transformation filter [eq. (14)] is applied to the model of vertical contact for comparison (Fig. 3 b). The initial value of impedance at the first iteration is given in terms of apparent resistivity (12.5 Ωm) and phase (50^o). The transformed apparent resistivity profile resembles that of VLF-R and exhibits smaller discrepance over the contact, indicating that improvement is made by this approach to the approximate solution filter (Fig. 6). However, to ensure a good estimate of H_y, a dense array of stations and a long profile are required[14], which would be impractical in the real field of measurement in the situation when only sparse and relatively short profile obtained. The dimensions of vertical grid in the FE algorithm used for this approach are mostly 25 m.

5. Application to field data

Two profiles of VLF-EM measurements have been chosen for the application of the filter. The profiles are located in sub-district of Baleendah south of Bandung, West Java. Two depth-sections of resistivity are available from 2D dc surveys using the Wenner-Schlumberger (WS) configuration for comparison. The profiles are bounded by

Citarum river to the north as shown in Fig. 7. The area is located within Bandung Basin, a large intramontane depression surrounded by volcanic highlands and characterized by lacustrine sediments[23]. The hilly topography surrounding the basin causes rivers in the rim of the basin flows into to the Citarum river, where during the high precipitation season flood frequently occurs around the investigated area. Clay, which has low permeability despite its high porosity is considered to partly causes the flood because it provides slow vertical drainage of water. Clayey top soil is observed visually in the field and the possibility of clay lenses existence at depth is also depicted by the dc resistivity cross-section (Fig. 7d and Fig. 8d).

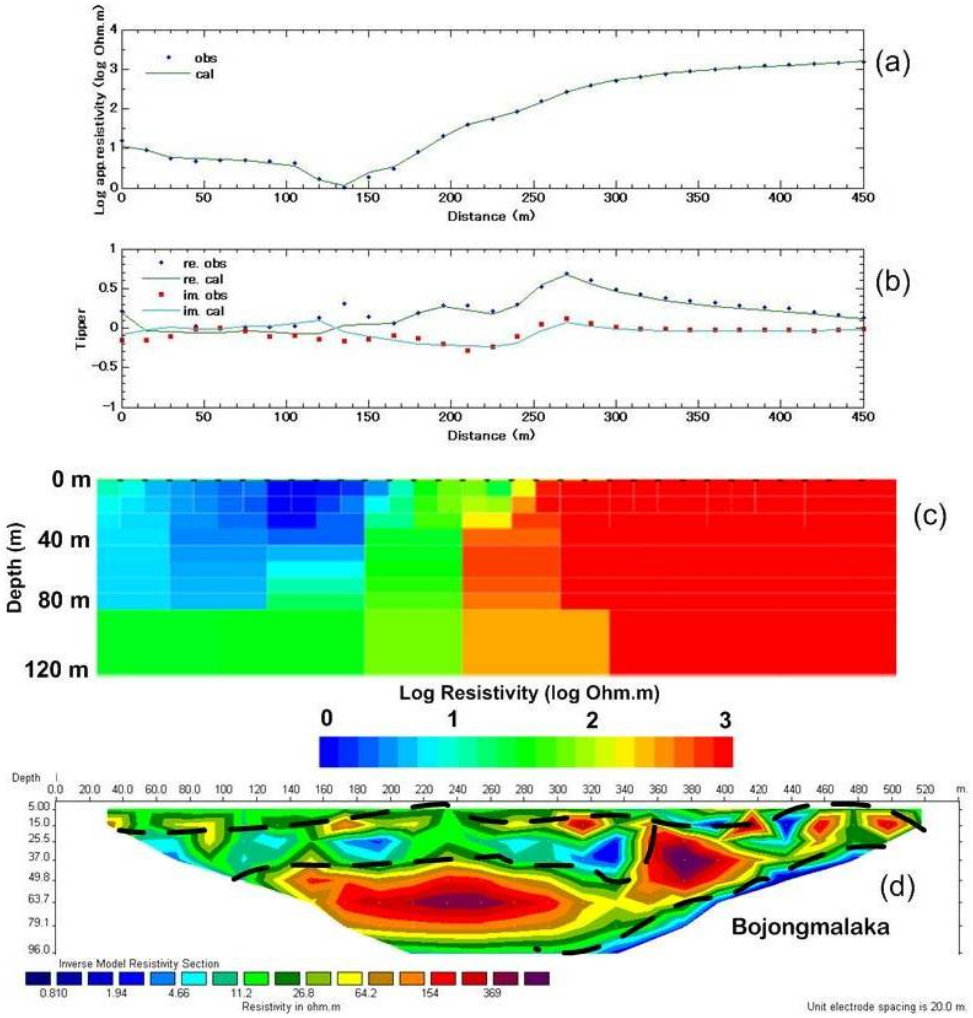

Figure 8. (a) Solid circles is the transformed apparent resistivity from the observed VLF signals in Line 2; solid line is the inverted apparent resistivity from the Occam inversion. (b) The observed real and imaginary components the tipper (solid circles and rectangles, respectively) and the calculated signal from the inversion (solid lines). (c) 2D resistivity model inverted from the observed tipper and apparent resistivity. (d) 2D resistivity model obtained from inversion of a 2D Wenner-Schlumberger configuration.

Line 1

Line 1 (Dayeuhkolot) is an W-E directed 450 m long VLF-EM profile surveyed in November 2005 at 19.8 kHz with spacing between stations of 15 m. The data along profile was 3-point averaged before processing. Transformation via the approximate solution was applied using an apparent resisitivity of 13 Ωm obtained from the dc resistivity measurement (30 m electrode spacing) as the initial value. The real and imaginary part of the tipper approximated from the measured in-phase and quadrature components are shown as solid circle and rectangle in Fig. 7b, whereas the transformed apparent resistivity in Fig. 7a (solid circle). Low value of apparent resistivity in the left side corresponds to the swamp around the stations. Higher apparent resistivity is observed to the right side of the profile which corresponds to drier surface environment.

To further evaluate the information contained in the transformed apparent resistivity and the observed tipper of the field data, a 2D Occam's inversion[24] was used to

jointly invert them into a 2D resistivity-depth section. The regularized non-linear inversion produces a smooth model that fits the data set within certain tolerances. The inverted model is presented in Fig 7c. The calculated apparent resistivity, and tipper from the last model of inversion after 40 iterations are also shown in Fig. 7a and Fig.7b, respectively. The minimum rms-misfit reached were 2.6 in the inversion. The observed (= transformed) apparent resistivity fits the calculated well, whereas discrepancy between the observed and calculated tipper is clearly observed, particularly the imaginary part. The dc resistivity-depth section (Fig. 7d) was obtained from inversion of WS configuration with 30 m electrode spacing, using Res2dinv code by Loke[25]. Compared to the dc resistivity-depth section, the shallow part of the section obtained from the VLF-EM signals exhibits almost similar feature. This is consistent with the VLF-EM ability to sense lateral variation of conductivity. However, the resistive shallow layer in Fig. 7c is almost one order of magnitude higher than the moderately resistive layer of the dc section. This might be related to the quality of the observed VLF-EM data that cannot be fitted well by the inverted data during the inversion, attributed to the small percentage of the observed signals. Two zone of conductive lenses which may indicate two zones of clay lenses depicted in the dc section (Fig. 7d) at 40 – 90 m depths can be identified in the resistivity section (Fig. 7c), on the other hand, their boundaries can not be resolved due to the smoothness constraint used in the inversion and the less depth resolution since it is only one value of frequency used in the inversion. Due to the latter reason, the resistive zone at depth in the middle of Fig. 7d is not sensed in the Fig. 7c.

Line 2

Line 2 (Bojongmalaka) is an S-N directed 450 m long VLF-EM profile surveyed in October 2005 at the same frequency of 19.8 kHz. The transformation was carried out with initial apparent resistivity value of 12.5 Ωm observed from the dc resistivity measurement. The same inversion method was applied to the VLF-EM signal and the transformed apparent resistivity. The observed and calculated responses are presented in Fig. 8a and Fig. 8b, and the inverted resistivity-dept section is shown by Fig. 8c. The rms-misfit reached after 60 iterations were 2.3. A better fitness between the observed and calculated data is obvious in this profile. Fig. 8d is the dc resistivity-depth section inverted from data with 20 m electrode spacing. The lateral distribution of resistivity in Fig. 8c is comparable to that of Fig. 8d. A conductive zone at shallow depth at the left side of line 2 in the dc section can also be observed in the inverted VLF-EM model as well as the tendency of increasing resistivity in the right side. Between the surface and the depth of 80 m, the vertical distribution of resisitivity also roughly mimics the dc resistivity.

6. Concluding remarks

In this study, numerical filters to transform the VLF-EM response (the tipper) into apparent resistivity along the profile of measurement have been carried out. The constructed filters are based on the formulation of approximate solution and full solution proposed by Chouteau et al.[13], and Gharibi and Pedersen[14], respectively. The filter has been tested using synthetic data for several basic models generated by a two-dimensional finite element modeling scheme. Good agreement between the apparent resistivity computed by the finite element algorithm and those yielded by the transformation filters was achieved, indicating that the filter is applicable for the actual field data.

The approximate solution filter was applied to two sets of field data. Further analysis was conducted by inverted the tipper and the transformed apparent resistivities into 2D resistivity-depth sections. The resulted sections were then compared to those inferred from 2D dc resistivity surveys. The inverted resistivity revealed the general features of the subsurface as compared with the dc resistivity results. It can be concluded that the lateral variation of resistivity is well resolved by the inverted model. To some extent, conductive zone beneath a resistive layer can be delineated by this workflow with bearing in mind the limitation of using just only one frequency in the inversion. More precise observation to the inverted models and the dc-resistivity model leads to suggestion that the VLF-EM data are less sensitive to small resistivity variations in a resistive environment. Nevertheless, the workflow in this study is very useful in improving the quantitative aspects of VLF-EM analysis. Considering the fact that VLF-EM survey is fast and inexpensive to deploy, this study can be regarded as a more integrated interpretation of VLF-EM data prior to using more expensive and time consuming methods such as VLF-R, dc-resistivity, seismic refraction/reflection, and CSAMT methods.

Acknowledgements

This research is partly funded by Research Grant ITB no: 0076/K01.03/PL2.1.5/VI/2005: *Electromagnetic induction methods for study of aquifer in South Bandung.*

References

1. Paal, G., *Ore prospecting based on VLF-radio signals*, Geoexploration, **3**, 139-145 (1965).
2. Fischer,G., Le Quang, B. V., and M¨uller, I., *VLF ground surveys, a powerful tool for the study of shallow two-dimensional structures*, Geophys. Prosp., **31**, 977–991 (1983).
3. McNeill, J. D., and Labson, V. F., *Geological mapping using VLFradio fields*, in : Nabighian, M. N., Ed., Electromagnetic methods in applied geophysics **II**. Soc. Expl. Geophys., 521–640 (1991).
4. Vozoff, K., *The effect of overburden on vertical component anomalies in AFMAG and VLF exploration*, Geophysics, **36**, 53–57 (1971).
5. Kaikkonen, P., *Numerical VLF modeling*, Geophys. Prosp., **27**,815–834 (1979).
6. Saydam, A. S., *Very low-frequency electromagnetic interpretation using tilt angle and ellipticity measurements*, Geophysics, **46**, 1594–1605 (1981).

7. Olsson, O., *Computation of VLF response over half-plane and wedge models*, Geophys. Prosp., **31**, 171–191 (1983).
8. Fraser,D. C., *Contouring of VLF-EM data*, Geophysics, **34**, 958–967 (1969).
9. Pedersen, L. B., Qian, W., Dynesius, L., and Zhang, P., *An airborne tensor VLF system: From concept to realization*, Geophys. Prosp., **42**, 863–883 (1994).
10. Karous, M., and S. E. Hjelt, *Linear filtering of VLF dip-angle measurements*, Geophy. Prosp., **31**, 782–794 (1983).
11. Ogilvy, R. D., and Lee, A. C., *Interpretation of VLF-EM inphase data using current density pseudosections*, Geophys. Prosp., **39**, 567–580 (1991).
12. Pedersen, L.B. and Becken, M., *Equivalent image derived from very-low-frequency (VLF) profile data*, Geophysics, **70**, G43-G50 (2005).
13. Chouteau, M., Zhang, P., and Chapellier, D., *Computation of apparent resistivity profiles from VLF-EM data using linear filtering*, Geophys. Prosp. **44**, 215-232 (1996).
14. Gharibi, M. and Pedersen, L.B., *Transformation of VLF data into apparent resistivities and phases*, Geophysics, **64,** 1393-1402 (1999).
15. Smith, B.D., and Ward, S. H., *On the computation of polarization ellipse parameters*, Geophysics, **39**, 867–869 (1974).
16. Paterson, N. R., and Ronka, V., *Five years of surveying with very low frequency–electromagnetics method*, Geoexpl., **9**, 7–26 (1971).
17. Cagniard, L., *Basic theory of the magnetotelluric method in geophysical prospecting*, Geophysics, **18**, 605–635 (1953).
18. Nabighian, M. N., *The analytic signal of two-dimensional magnetic bodies with polygonal cross-section: Its properties and use for automated interpretation*, Geophysics, **37**, 507–517 (1972).
19. Jin, J-M., *The finite element method in electromagnetics*, Willey, New York, 1993.
20. Press, W. H., Flannery, B. P., Teukolsky, S. A., and Vetterling, W. T., *Numerical recipes in Fortran—The art of scientific computing*, Cambridge Univ. Press, 1996.
21. Srigutomo, W and Sutarno, D., *2D electromagnetic modeling for a plane wave case*, Kontribusi Fisika Indonesia, **9:2,** (in Bahasa with English abstract) (1998).
22. Sutarno, D. And Srigutomo, W., *Application of the finite element method in 2D electromagnetic modeling for a line source excitation*, Kontribusi Fisika Indonesia, **9:3,** (in Bahasa with English abstract), (1998).
23. Dam, M.A.C., Suparan, P., Nossin, J.J., Voskuil, P.G.A., *Achronology for geomorphological developments in the reater Bandung area, West-Java, Indonesia*, J. Southeast Asian Earth Sci. **14** (1–2) , 101–115 (1996).
24. deGroot-Hedlin, C., and Constable, S., *Occam's inversion to generatesmooth two-dimensional models from magnetotelluric data*, Geophysics, **55**, 1613–1624 (1990).
25. Loke, M. H., Res2dinv software user's manual 1997.